Impact of thermal history on defects formation in the last solid fraction of Cz silicon ingots

Adeline Lanterne, Guilherme Gaspar, Bjørn Haave, Moez Jomâa, Rune Søndenå, Alexander Hupfer, Yu Hu, and Marisa Di Sabatino

Citation: AIP Conference Proceedings **1999**, 130012 (2018); doi: 10.1063/1.5049331
View online: https://doi.org/10.1063/1.5049331
View Table of Contents: http://aip.scitation.org/toc/apc/1999/1
Published by the American Institute of Physics

Articles you may be interested in

Simple modeling of intrinsic bulk lifetime in doped silicon
AIP Conference Proceedings **1999**, 020003 (2018); 10.1063/1.5049242

Influence of temperature on light induced phenomena in multicrystalline silicon
AIP Conference Proceedings **1999**, 130007 (2018); 10.1063/1.5049326

Role of hydrogen: Formation and passivation of meta-stable defects due to hydrogen in silicon
AIP Conference Proceedings **1999**, 130010 (2018); 10.1063/1.5049329

Resistivity profiles in multicrystalline silicon ingots featuring gallium co-doping
AIP Conference Proceedings **1999**, 130016 (2018); 10.1063/1.5049335

A novel approach for suppression of oxygen precipitation in CZ silicon wafers of solar cells by pre-thermal treatment
AIP Conference Proceedings **1999**, 130018 (2018); 10.1063/1.5049337

Influence of dielectric layers and thermal load on LeTID
AIP Conference Proceedings **1999**, 130020 (2018); 10.1063/1.5049339

AIP | Conference Proceedings
Enter Promotion Code PDF30 at checkout
Get 30% off all print proceedings!

Impact of Thermal History on Defects Formation in the Last Solid Fraction of Cz Silicon Ingots

Adeline Lanterne[1, 2, a)], Guilherme Gaspar[1, 3], Bjørn Haave[1], Moez Jomâa[4], Rune Søndenå[5], Alexander Hupfer[6], Yu Hu[7] and Marisa Di Sabatino[1]

[1]*Dept. Materials Science and Engineering, NTNU, Alfred Getz vei, 2B, 7491 Trondheim, Norway*
[2]*CEA - INES, 50 avenue du lac Léman, F-73375 Le Bourget du Lac, France*
[3]*Dept. of Physics - I3N, University of Aveiro, 3810-193 Aveiro, Portugal*
[4]*SINTEF Industry, Instituttveien 18, 0314 Oslo, Norway.*
[5]*Institute for Energy Technology, P.O. Box, N-2007 Kjeller, Norway*
[6]*Dept. of Physics, University of Oslo, Gaustadalléen 23C, MiNaLab, 0373 Oslo, Norway*
[7]*NorSun AS, Årdal Plant, P.O. Box 104, 6881 Årdalstangen, Norway*

[a)]Corresponding author: adeline.lanterne@cea.fr

Abstract. For the first time, the impact of the tail detachment on the quality of the last solid fraction of a Czochralski silicon ingot body is reported. Simulations of the thermal history were performed on CGSim software and showed that producing an ingot with a tail detached from the melt before the cone-end (the so called "*popped-out*" tail) changes the time that the last part of the ingot body remains at the 900-1200°C temperature range and could thus impact the growth of defects such as oxygen precipitates. In addition, ingots with tails completely grown were characterized and compared to ingots with popped-out tails. Lifetime measurements of the ingot last solid fraction were performed while voids and oxygen related defects were delineated with chemical etchants. These measurements were complemented with FTIR measurements performed at room and low temperature (30 K), before a two-step thermal oxidation took place. The results show no impact of the earlier detachment from the melt on the as-grown lifetime, as long as the generation and propagation of dislocations due to the detachment are constrained inside the tail. However, after the thermal oxidation, lower oxygen stacking fault density is found in the popped-out ingots, highlighting a possible improvement of the Czochralski quality with shorter tails.

INTRODUCTION

The development of high efficiency silicon solar cells, with advanced structures such as HIT and IBC cells, requires the use of high quality Czochralski (Cz) monocrystalline silicon wafers [1]. The understanding of the defects formation during the Cz silicon growth is crucial to better control and improve the quality of this material.

In this study, we focused our research on the last 10 cm of the ingot body, just before the growth of the tail, where few studies have been carried out in the literature. In this ingot region, a different thermal history can be found compared to the rest of the body due to the growth of the tail and due to the ingot detachment from the remaining melt. As this detachment can sometimes happen earlier than planned in industry (before the complete growth of the tail), it becomes important to study its impact on the quality of the last ingot solid fraction. The so-called "popped-out" ingots, with a shorter tail, should then have then a different thermal history, which is expected to have a direct impact on the defect formation in the ingot main body [2].

The thermal history of such ingots was simulated along with the characterization of three industrial Cz silicon ingots with various tail lengths.

SiliconPV 2018, The 8th International Conference on Crystalline Silicon Photovoltaics
AIP Conf. Proc. 1999, 130012-1–130012-8; https://doi.org/10.1063/1.5049331
Published by AIP Publishing. 978-0-7354-1715-1/$30.00

SIMULATIONS AND EXPERIMENTS

Simulation of the Cz Ingot Thermal History

The thermal history of Cz silicon ingots with different tail shapes were simulated in order to quantify the thermal budget and cooling rate variations in the last 10 cm of the ingot body. Both ingots with a tail completely grown up to the cone-end and a popped-out tail were compared.

The software Crystal Growth Simulator (CGSim) developed by STR Group was used for this simulation [3]. It is based on the finite volume analysis for the optimization of partial differential equations. As input, the chamber geometry is specified as a 2D setup with circular symmetry, along with details about the materials, the heater elements, and several process parameters and assumptions [4]. The ingot temperature was simulated during the solidification of the whole ingot and then after its detachment from the melt, during the pulling and ingot stay in the receiving chamber (cooling chamber). In the simulation, the heaters are turned off right after detachment. The furnace geometry and the others inputs correspond to the puller used to grow of the ingots that were characterized in this work.

Characterization of Lifetime and Defects

To study the consequences of the temperature variation observed in the simulations, three Cz silicon ingots with different tail lengths were investigated: a first ingot with a complete tail of 12 cm, called *Reference,* and two popped-out ingots, called *Popped-out 1* and *Popped-out 2,* detached from the melt 8 cm and 7 cm after the beginning of the tail growth stage, respectively. The shape of the different tails can be seen in the schematics of Fig. 1 along with the last 10 cm of the ingot body.

The three characterized ingots are n-type (phosphorus doped) ingots grown in an industrial scale Cz puller dedicated to photovoltaic (PV) applications. They were chosen to have different tail shapes as well as similar resistivity and similar impurities concentrations such as interstitial oxygen [O_i] and substitutional carbon [C_s] (see discussion of Table 1 below).

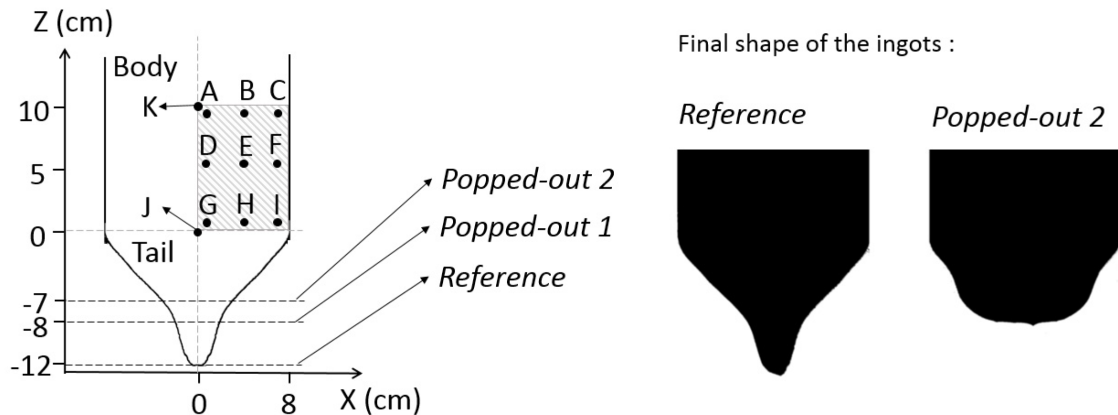

FIGURE 1. Schematics of the ingot cross section showing the cutting of vertical slabs (striated area) and the different tail lengths. Point A to I correspond to the positions where measurements were performed. Point J and K correspond to position used for the simulation of thermal history. The final shapes of *Reference* and *Popped-out 2* ingots are shown on the right-hand side of the figure.

To be able to characterize these ingots, they were cut at approximately 10 cm above the beginning of the tail. Several 2 mm thick slices were then cut parallel to the growth direction from the central axis to the ingot edge, as shown in Fig.1 (striated area). After cutting, all the slices were mechanically polished.

The [O_i] and [C_s] were measured on each ingot by Fourier transform infrared spectroscopy (FTIR) using the SEMI standard F1188. Measurements were performed at NTNU on 9 points of the slice (points A to I in Fig. 1).

Average results and variations are shown in Table 1 along with the resistivity performed on the same position by the four point probe (FPP) method.

All the three ingots are in the same resistivity range, the variation from 3.6 to 4.1 Ohm.cm being not significant for industrial PV n-type ingots as compared to the possible variation along a single ingot [5]. The average [O_i] concentration gives a first indication that the three samples have similar values, all under low [O_i] regime for this type of Cz ingot. The variation from 11.2 to 12.7 ppma is negligible compared to the samples variations. Finally, the [C_s] is low for all ingots and close to the detection limit of the instrument.

TABLE 1. Resistivity, interstitial oxygen [O_i] and substitutional carbon [C_s] concentrations (before and after thermal oxidation) of the three studied ingots. The presented values correspond to the average value and between the 9 points measured on the slabs, point A to I presented in Fig. 1 with the variation.

Ingots	Resistivity [Ohm.cm]	As-grown [Oi] [ppma] (σ)	[Cs] As-grown [ppma] (σ)	[Oi] After oxidation [ppma] (σ)	[Cs] After oxidation [ppma] (σ)
Reference	3.8 ± 0.4	11.2 ± 1.2	0.8 ± 0.2	11.1 ± 1.2	0.8 ± 0.2
Popped-out 1	4.1 ± 0.3	12.7 ± 1.7	0.6 ± 0.1	12.7 ± 1.9	0.6 ± 0.1
Popped-out 2	3.6 ± 0.3	11.9 ± 2.0	1.1 ± 0.5	11.8 ± 1.8	1.1 ± 0.1

Two methods were used to investigate the minority carrier lifetime of as-grown samples. Initially, it was measured on the ingot blocks cross section, before to being cut into slabs, with a Sinton BCT-300 tool in transient photoconductive decay (PCD) mode. On each block, the lifetime was measured along the ingot central axis at Z=0; 5 and 10 cm (see Fig. 1) for a fixed carrier injection level of $5.0x10^{14}$ at/cm^3. After mechanical polishing, the minority carrier lifetime distribution of each ingot was measured (at the slab level) by the carrier density imaging (CDI) technique without passivation. The CDI was set to the emission mode at 80˚C [6] and the lifetime was obtained by imaging the excess free carrier density under the illumination of two lasers with a wavelength of 940 nm each [7].

FTIR at low temperature (30 K) was used to investigate the oxygen related defects on *Reference* and *Popped-out 2* ingots. The measurements were performed at the University of Oslo on as-grown vertical slices at the very same position from the tail: D position in Fig. 1.

To reveal the flow pattern defects (FPD), which are normally associated to voids formation during ingot cooling, a vertical slice from each block was cleaned in a RCA1 solution (H_2O_2:NH_4OH:H_2O, 1:1:5 parts) and etched with a Secco etching for 30 min without agitation [8]. Etch pits were formed showing the nuclei site along with flow pattern of 100 µm to 1 mm. FPD were then investigated with optical microscopy (OM) and their density determined.

In order to precipitate and grow oxygen-related defects for better visualization, a two-step oxidation heat treatment was performed on one parallel slab from each ingot. The oxidation treatment include a first nucleation step at 750°C for 4 hours followed by a precipitation step at 1050°C for 16 hours.

After oxidation, [O_i] and [C_s] were measured again in the same 9 positions as before oxidation (see Table 1). The oxygen induced stacking faults (OiSF) were then revealed by using Wright etching [9] and observed by OM.

Finally, and in order to obtain the minority carrier lifetime on the heat treated slices, an etching of 3 min in a CP5 solution (HNO_3:HF:CH_3COOH, 10:2:5 parts) was used followed by a cleaning step in Piranha solution (H_2SO_4:H_2O_2, 5:1 parts). The samples were then double-side passivated using hydrogenated amorphous silicon (a-Si:H) deposited with PECVD and the minority carrier lifetime distribution measured with photo-luminescence imaging [10].

RESULTS AND DISCUSSION

Cooling Rate Variation

The thermal history of the *Reference* and *Popped-out 2* ingots were simulated to evaluate the differences in the last body fraction between an ingot with a fully grown tail and an ingot with a popped-out one. The thermal history was simulated in positions J and K (see Fig. 1) to cover the last 10 cm of ingot body. The temperature of each

position was simulated from the time of its solidification to the end of the tail growth and further during the ingot cooling. The thermal history of the two specified positions, for both *Reference* and *Popped-out 2* ingots, are shown in Fig. 2, where (1) represents the start of the tail (same for both ingots) and (2) and (3) the moment when each of the corresponding ingots are detached from the melt. 0 in the horizontal axis represents the time where point K is solidified and as such it is represented by the melting point temperature of silicon.

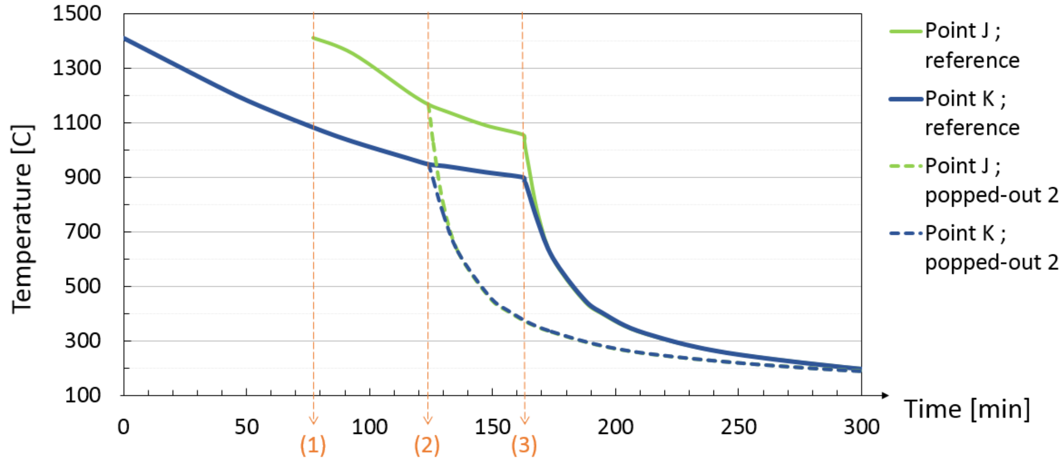

FIGURE 2. Temperature simulation of the Cz silicon ingots on CGSim software, from the solidification of the last 10 cm of ingot body to the end of the cooling. With (1) corresponding to the begging of the tailing growth stage, (2) and (3) the detachment from the melt in the *Popped-out 2* and *Reference* case, respectively. Point J and K are specified in Fig. 1.

Results in Fig. 2 highlight the possibility of dramatically change the time that the ingot is kept in the 900 - 1200°C temperature range. In position J, for instance, this time decreases from approximately 50 min for the *Reference* tail to approximately 12 min for the *Popped-out 2* tail. This temperature range is important for the voids formation but also for the stability of oxygen precipitate nuclei [11].

Lifetime Measurements in As-grown Condition

The results of the as-grown lifetime measurements on the blocks cross section by transient-PCD are shown in Fig. 3a.

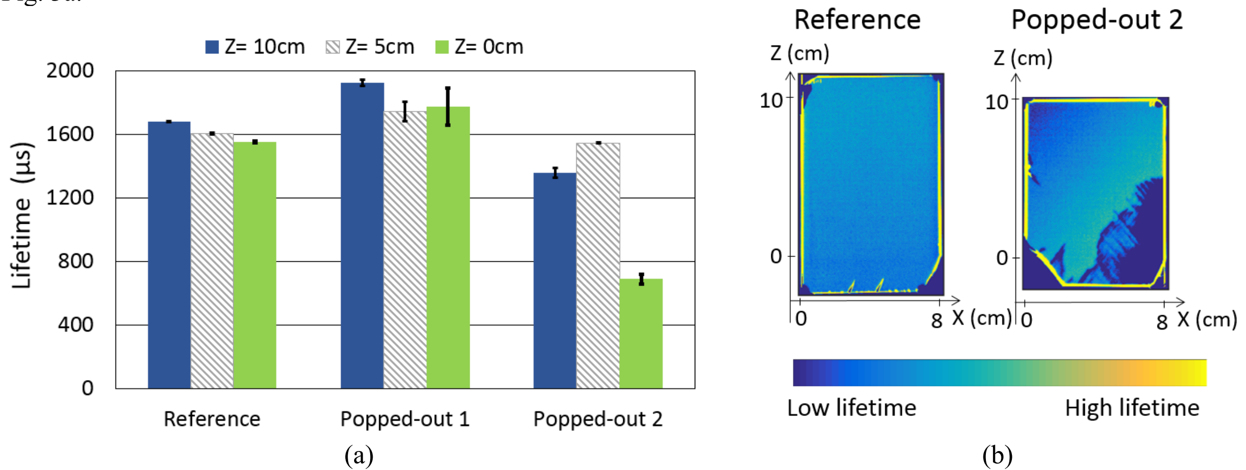

FIGURE 3. (a) As-grown transient-PCD lifetime measured at the block level at 0, 5 and 10 cm from the tail and along the central axis of each ingot. (b) As-grown CDI lifetime images of slabs for *Reference* and *Popped-out 2* ingots as represented in Fig.1. Ingot edge corresponds to X=8 cm, ingot center to X= 0 cm and the body end to Z=0 cm.

Similar lifetime can be found in the last 10 cm of the Cz body for the *Popped-out 1* and *Reference* ingots. A slightly lower lifetime is measured in *Popped-out 2* ingot at 10 cm and 5 cm before the tail compared to *Popped-out 1* ingot. As the low [O_i] and [C_s] values (cf. Table 1) cannot explain this decrease one hypothesis could be a difference in the metallic impurity content compared to the two other ingots under investigation.

At the end of the body (Z=0 cm) in *Popped-out 2* ingot, a significant decrease of the lifetime is measured: 700 µs compared to the 1400-1500 µs at 5 and 10 cm before the tail. One explanation for this lower lifetime can be seen in Fig. 3b where the as-grown lifetime was measured on 2 mm thick slabs by CDI. While the lifetime is homogenous in the whole sample area for the *Reference* ingot, an area with lower lifetime can be seen in the last 5 cm of body and closer to the outer part of the *Popped-out 2* ingot. This corresponds to a region of slip dislocation lines [12]. These dislocations are the consequence of the sharp detachment from the melt. Following the thermal shock, dislocations can propagate backward in the ingot body over several centimeters either from the solid/liquid interface or the ingot edge [13]. They are also found in the tail part of the *Popped-out 1* ingot; however they do not propagate into the body region due to the differences in the tail shape as a smaller ingot section was in contact with the melt at the moment of the detachment.

To conclude on the as-grown lifetime, excluding the areas where dislocations propagate, the earlier detachment from the melt does not seem to impact the ingot lifetime under as-grown conditions despite the thermal history variation observed in the simulation section.

Defects Investigation in As-grown Ingots

1) Flow Pattern Defects (FPD)

Examples of FPD observed in the three ingots are shown in Fig. 4 for the case of the *Popped-out 1* ingot. Similar FPD densities were found between the *Reference* and the two popped-out ingots with a value ranging from 250 to 300 cm^{-2}. In all of them, a lower FPD density was found close to the ingot edge as it can be seen in Fig. 4c. Thus, as for the as-grown lifetime, no impact of the earlier detachment from the melt can be detected at the voids level.

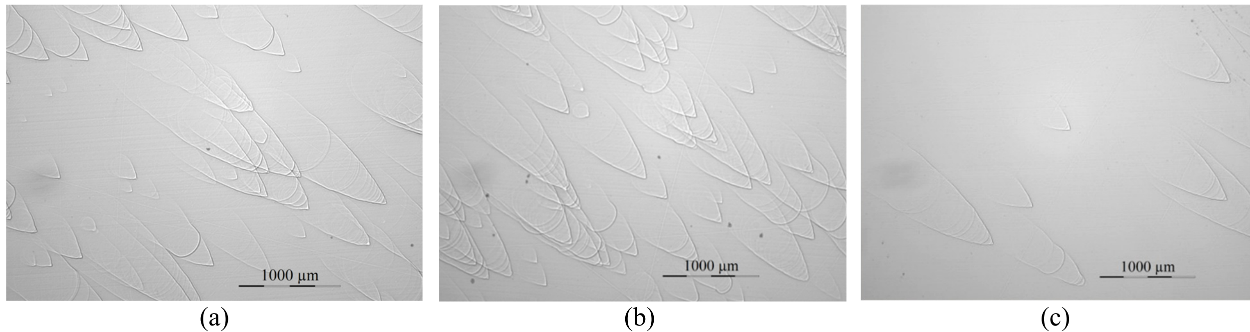

FIGURE 4. Example of OM observations from the sample surface after Secco etching for the *Popped-out 1* ingot. Voids or D-defects are found as pits in the corner of the V-shaped etched features (flow pattern defect). (a), (b) and (c) correspond to position D, E and F in the slice, respectively (see position in Fig. 1).

2) Study of Oxygen-Based Defects by Low Temperature FTIR

In addition FTIR at low temperature (30K) were performed on the as-grown samples in order to study the oxygen defects before the thermal oxidation. Results of the local measurements in point D of ingots *Reference* and *Popped-out 2* are shown in Fig. 5. A higher O_i peak at 1135 cm^{-1}, in respect to the corresponding spectrum baseline, is found in the *Reference* ingot compared to *Popped-out 2*.

In Table 1, it is possible to see that both ingots have similar [Oi] values close to the tail, with an average on the slice a slightly higher for *Popped-out 2* ingot. It should be noted that important radial variations are found in these slices as well as a higher [Oi] in the dislocated area of *Popped-out 2*. In position D, however, a lower O_i peak at 1135 cm^{-1} is measured for the popped-out tail.

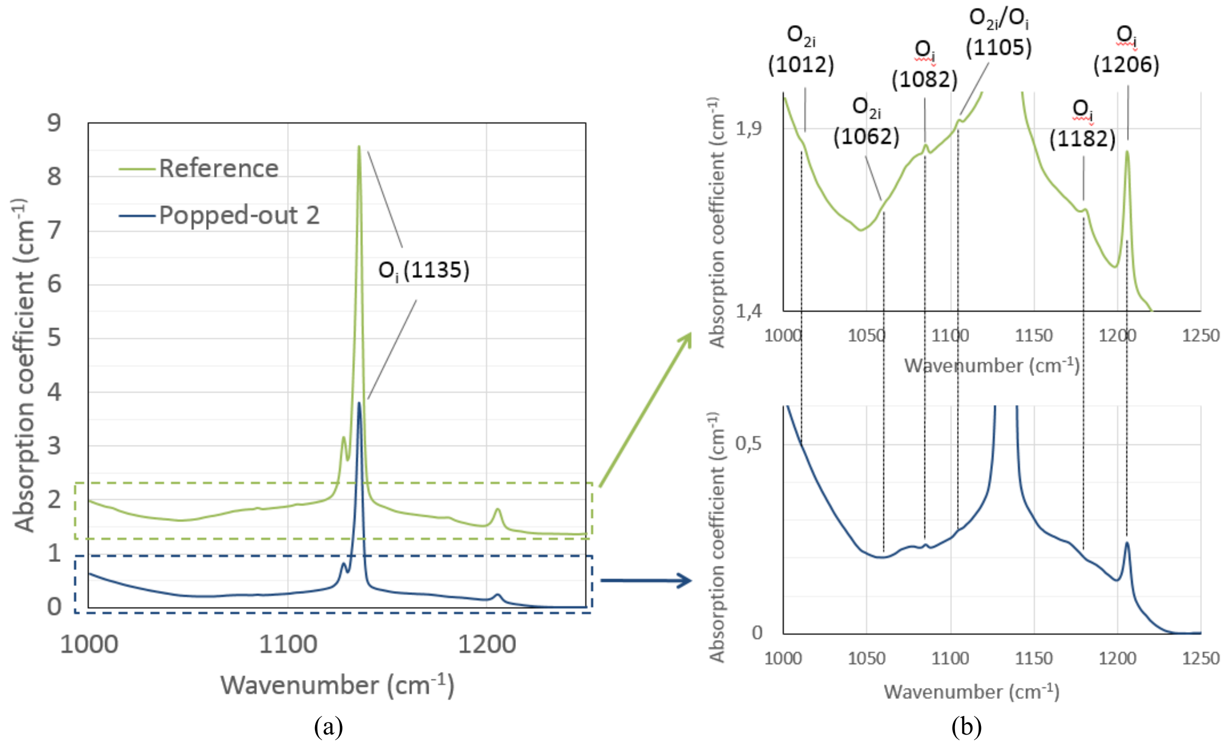

FIGURE 5. (a) FTIR measured at 30K at Point D, as shown in Fig. 1, for the *Reference* and *Popped-out 2* ingots. (b) Zoom of the FTIR curve highlighting the main O_{2i} and O_i signals (1000-1250 cm^{-1}).

The oxygen dimer, O_{2i}, results from the diffusion and agglomeration of two interstitial oxygen atoms in the silicon matrix. They are known to be one of the sources of thermal donors formation [14] and thus it becomes important to detect their presence in the context of this work. They show several vibrational bands when excited with an IR source, namely at 1012 and 1060 cm^{-1} [15]. The low temperature FTIR spectrum of the *Reference* ingot shows signs of these peaks; however in the *Popped-out 2* ingot, no O_{2i} peaks can be found at these wavenumbers highlighting a noticeable difference between the two ingots in addition to the simulated cooling rates variation.

Defects Investigation after Thermal Oxidation

FTIR measurements of $[O_i]$ and $[C_s]$ after thermal oxidation are shown in Table 1. No variation of the $[O_i]$ concentration was measured after oxidation for the three ingots, as the decrease of 0.1 ppma found for both the *Reference* and *Popped-out 2* ingots is close to the detection sensitivity of FTIR. This absence of variation highlights the low quantity of oxygen precipitates that may form in further processing steps with some thermal budget involved in. Even if few precipitates seem to be formed, the lifetime was imaged after oxidation and the oxygen precipitates were delineated to look into more detail at the differences according to the noticeable thermal history.

1) PL Lifetime Imaging

The PL images of the vertical slabs, after thermal oxidation, are shown in Fig. 6. Homogeneous minority carrier lifetime is observed on the last 10 cm of ingot body in the *Reference* and *Popped-out 1* samples. The lower lifetime patterns at the top of *Reference* sample (straight lines in two directions) correspond to cracks that develop during the cutting of the slice. In *Popped-out 2* sample, a homogeneous lifetime is also measured except in the dislocation area, on the bottom right-hand side area of the sample, where the lifetime is lower.

Since the lifetime has demonstrated to be relatively homogeneous in all the three ingots, we can conclude on the absence of lifetime degradation due to oxygen precipitation during the thermal treatment. This is in agreement with

the absence of [O_i] variation during the thermal oxidation as well as with the low [O_i] levels measured on these ingots (cf. Table 1).

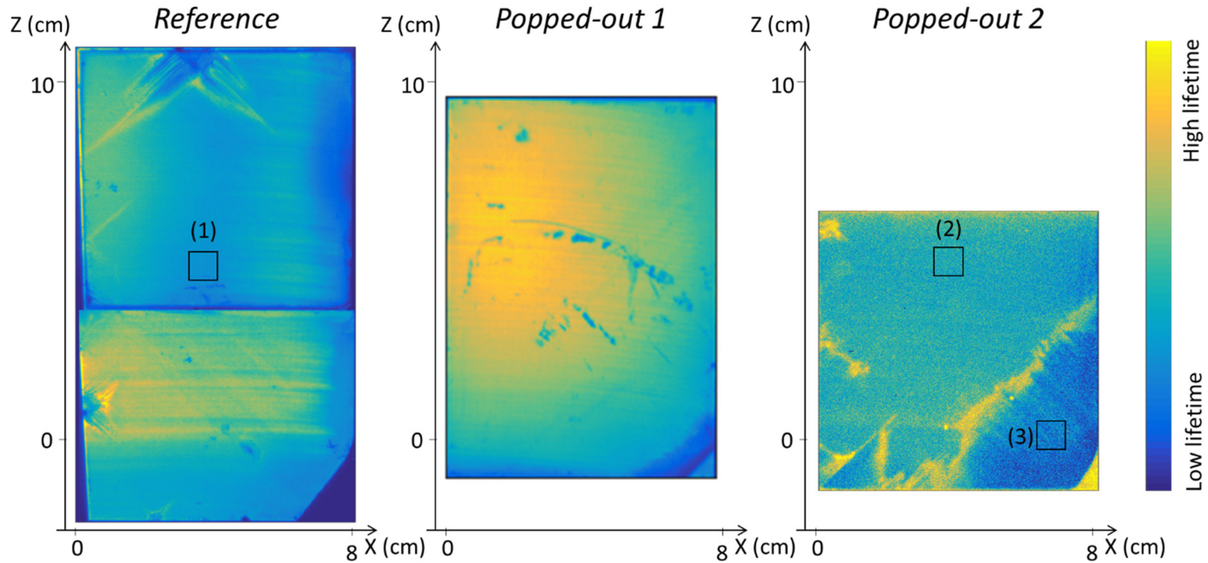

FIGURE 6. Uncalibrated PL lifetime maps of 2 mm passivated slabs (see cutting in Fig. 1) after thermal oxidation. Ingot edge corresponds to X=8 cm, ingot center to X= 0 cm and the body end to Z=0 cm. (1), (2) and (3) correspond to position where the OiSF were investigated by OM. Remarque: the scale varies between the samples.

2) Oxygen Precipitates and Stacking Faults (OiSF)

Figure 7 shows the defects revealed by Wright etching on the oxidized samples. By comparing Fig. 7a and Fig. 7b, a lower density of OiSF is found in the *Popped-out 2* ingot compared to the *Reference* one. Fig. 7a and Fig. 7b were performed at the position E on the slices (see Point E in Fig.1). For each ingot, similar OM micrographs were obtained at positions A, B and D (shown in Fig. 1) than in position E. In all of them, a lower OiSF density was confirmed for the *Popped-out 2* compared to the *Reference*. On the other side, a very high density of OiSF was found in the region containing dislocations in *Popped-out 2* (Fig. 7c). Excluding the area with dislocations, the lower OiSF density was also confirmed in two other popped-out ingots similar to *Popped-out* 2 as compared to the *Reference* ingot (not shown in this paper).

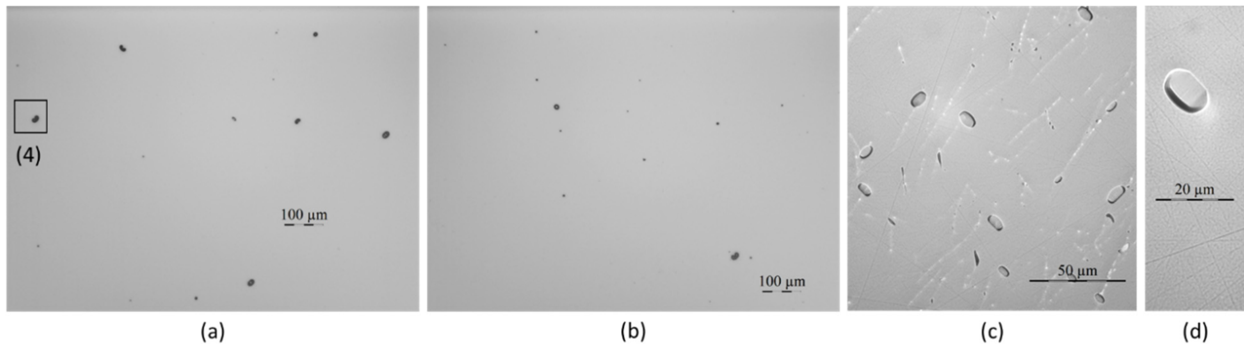

FIGURE 7. (a), (b) and (c) OM micrographs after Wright etching of thermally oxidized slabs in position (1), (2) and (3) shown in Fig. 6, respectively. Positions (1) and (2) are similar to point E in Fig. 1. (d) Zoom of one OiSF etch pits shown in Fig. 7a in position (4).

The lower OiSF density observed in the *Popped-out 2* ingot could be related to the lower concentration of O_{2i} measured in the as-grown condition along with the lower O_i peaks at 30 K in this sample. Moreover, as the formation of oxygen-related defects greatly depend on the thermal history of the sample, the differences observed in OiSF concentration between the *Reference* and *Popped-out 2* ingots could be a consequence of the differences in thermal history discussed in the simulation section.

CONCLUSION

The results show no impact of the earlier detachment from the melt on the as-grown lifetime, as long as the generation and propagation of dislocations due to the detachment are constrained inside the tail. In addition, no impact of the tail length on voids density was found. After a thermal oxidation, very few oxygen defects were found in these low oxygen concentration ingots. However, a lower oxygen stacking fault density was observed in the popped-out ingots, in agreement with lower O_i and O_{2i} peak intensities measured using low temperature FTIR before oxidation. In addition, simulations of the thermal history on CGSim software were performed and showed that producing an ingot with a popped-out tail can change the time that the last part of the ingot body is subject to temperatures between 900°C and 1200°C, which indeed can impact the growth of oxygen-related defects during crystal cooling.

ACKNOWLEDGMENTS

The authors would like to thank the 'Norwegian Research Centre for Solar Cell Technology' (contract number 193829), centre co-sponsored by the Norwegian Research Council and research and industry partners in Norway, for the financial support.

REFERENCES

1. R. Kopecek and Joris Libal, Photovoltaic International, 1-7 (2013).
2. V.V. Voronkov, Mat. Science and Engineering: B **73,** (1–3), 69–76 (2000).
3. http://www.str-soft.com/products/CGSim/
4. O. Asadi Noghabi, M. M'Hamdi and M. Jomâa, Meas. Sci. Technol. **24,** 015601 (2013).
5. B. Martel et al. "Influence of the wafer position within a n-type monocrystalline ingot on the conversion efficiency" presented at the nPV Workshop, Konstanz (2015).
6. M. C. Schubert, J. Isenberg, and W. Warta, J. Appl. Phys. **94**, (6), 4139–4143 (2003).
7. M. Bail, J. Kentsch, R. Brendel, and M. Schulz, 28th IEEE Photovolt. Spec. Conf. pp. 99–103 (2000).
8. W. Wijaranakula, J. Electrochem. Soc. **141**, 3273-3277 (1994).
9. M.W. Jenkins, J. Electrochem. Soc. **124**, 757-762 (1977).
10. T. Trupke, et al., App.Phys. Lett. **89** (4), 044107 (2006).
11. Y. Shimanuki, H. Furuya, and I. Suzuki, J. Electrochem. Soc. **136** (7), 2058-2062 (1989).
12. W. Zulehner, J. of Crystal Growth **65,** 189-213 (1983).
13. A. Lanterne et al. J. of Crystal Growth, **458,** 120-128 (2017).
14. W. Kaiser, Phys. Rev, **105** (6), 1751-1756 (1957).
15. L. I. Murin, T. Hallberg, V. P. Markevich and J. L. Lindstrom, Physical review letters **8** (1998).